

Equilibration in an Eddy Resolving Model with Simplified Physics*

AMY SOLOMON

International Pacific Research Center, SOEST, University of Hawaii at Manoa, Honolulu, Hawaii

PETER H. STONE

Department of Earth, Atmospheric and Planetary Sciences, Massachusetts Institute of Technology, Cambridge, Massachusetts

(Manuscript received 6 July 1999, in final form 28 June 2000)

ABSTRACT

The role of waves in maintaining the midlatitude tropospheric climate is investigated in a dry high-resolution quasigeostrophic β -plane channel model coupled to both a simplified model of the atmospheric boundary layer and an interactive static stability.

The climate of the model's equilibrated state is found to be separated into two dynamical regimes, one within the boundary layer and the other within the free troposphere. Thermal diffusion in the atmospheric boundary layer prevents the eddies from modifying the mean temperature structure there by damping temperature fluctuations. The potential vorticity gradients are essentially eliminated in the lower troposphere above the boundary layer, in agreement with observations. The homogenization of potential vorticity occurs in the region where the baroclinic waves have a critical layer, and is accomplished mainly by an increase in the static stability in the lower troposphere due to the vertical eddy heat fluxes.

Even though the model has kinetic energy and enstrophy spectra characteristic of a fully turbulent flow, the equilibrated state of the model is essentially maintained by wave-mean flow interaction, primarily by the interaction between wave 5 and the zonal mean state. The zonal mean of the equilibrated state is found to be linearly stable to all waves. The largest-scale wave in the fully nonlinear state, wave 4, is found to be maintained by an energy cascade from the higher wavenumbers. However when wave 4 is large, stability analysis indicates that it is unstable, with the growing mode dominated by wave 6. This instability appears to saturate quickly and hand its energy over to wave 5. The result is that the amplitude of waves 4 and 5 in the equilibrated state are strongly anticorrelated, but the fluctuations in total eddy kinetic energy are strongly correlated with the fluctuations in the sum of the energy in waves 4 and 5.

1. Introduction

The Charney–Stern criterion for instability is a necessary condition for instability but it is not sufficient. A basic state that has a change of sign in the meridional gradient of potential vorticity may be stable. A linear stability analysis of the equilibrated state proposed by Lindzen (1993) shows that the baroclinic normal modes have been stabilized even though this state still satisfies the Charney–Stern necessary condition for instability.

The equilibrated state proposed by Lindzen (1993) is

consistent with the observational studies of Fullmer (1982), Sun and Lindzen (1994), and Morgan (1994), which have shown that the potential vorticity gradients in the extratropics are significantly less than β , the meridional gradient of planetary vorticity, in the midtroposphere but large in the planetary boundary layer and a maximum at the tropopause. Stone and Nemet (1996) have argued that this vertical structure is consistent with a layer of strong baroclinic adjustment in the lower troposphere, separating layers with relatively little baroclinic adjustment in the boundary layer and in the upper troposphere. In these studies it was found that the observed extratropical temperature structure is determined, in part, by the mixing of potential vorticity along isentropic surfaces and that the impact of this mixing varies considerably in the vertical.

In order to resolve realistic neutral states, then, it appears that it is necessary to allow the dynamical balance at the surface, in the midtroposphere, and at the tropopause to vary. A two-level model couples the dynamics in the lower troposphere with the upper tropo-

* School of Ocean and Earth Science and Technology Publication Number 5308 and International Pacific Research Center Publication Number 56.

Corresponding author address: Dr. Amy Solomon, International Pacific Research Center, SOEST, University of Hawaii at Manoa, 1000 Pope Road, Honolulu, HI 96822.
E-mail: amy@iprc.soest.hawaii.edu

sphere. This causes the dynamics at the jet and the dynamics in the boundary layer to interact in a very artificial way, and the equilibrated state of the two-level model may have very little to do with the observed climate. If the dynamics in the observed climate are roughly approximated by the state hypothesized by Lindzen (1993), a model with more than two levels would be necessary to resolve it.

This process model study attempts to construct a model adequate to resolve a neutral state that is relevant to the atmosphere. This model is used to illustrate the importance of the coupling between the quasigeostrophic dynamics in the free troposphere and the dynamics in the atmospheric boundary layer (ABL) in maintenance of the equilibrated state. Since the interaction between surface heat fluxes, static stability, and vertical eddy heat fluxes makes an important contribution to the eddy–mean flow interaction (Stone 1972; Gutowski et al. 1989), we include an interactive static stability in our model. The extent to which potential vorticity is homogenized is explored and discussed in light of current theories about the nonlinear equilibration of the observed midlatitude troposphere. This issue is motivated by the study of Lindzen (1993), which hypothesized that a possible simplistic equilibrated state that describes the observed midlatitude troposphere is a state where the potential vorticity gradients in the midtroposphere have been homogenized such that waves propagating along the tropopause and the surface of the earth can no longer interact.

Section 2 describes the model used in this study. Section 3 demonstrates the adequacy of the model's resolution and domain size. Section 4 compares the equilibrated state of the model to observations. Section 5 discusses the evolution of the model's climate to the equilibrated state. Section 6 discusses the role of wave–wave and wave–mean flow interactions in the equilibrated state. Section 7 discusses the stability characteristics of the equilibrated state. Section 8 discusses the implications of these results for wave–mean flow interaction in equilibrated states similar to the atmosphere's.

2. The model

The model used in this study integrates the quasigeostrophic equations coupled to an equation for the horizontally averaged potential temperature on a midlatitude β plane. The model has variable vertical and horizontal resolution. The zonal, meridional, and vertical coordinates are evaluated in gridpoint space. Grid points in the vertical are equally spaced as a function of pressure. There is a rigid lid in pressure coordinates at the top and bottom of the model. There is no flow through the channel walls, and periodic boundary conditions are applied to all fields in the zonal direction.

All runs are initially in radiative–convective equilibrium (RCE). The model is run for 20 days without a perturbation to allow the dynamics in the planetary

boundary layer to approach an equilibrium consistent with RCE. Then the model is perturbed with small-amplitude waves 1–9. The amplitude of the pressure perturbation at the surface is 10 Pa in each of the nine waves.

The standard run (SR) has a channel width of 10 000 km and a channel length of 21 040 km. The channel width is approximately 90° in latitude and was chosen in order to prevent the dynamics at the channel walls from modifying the dynamics at the center of the channel. The horizontal resolution is equal in both the zonal and meridional directions and is set equal to 300 km in the standard run. The standard run has 17 equally spaced vertical levels.

a. Model equations

This model integrates the quasigeostrophic potential vorticity equation in pressure coordinates:

$$\frac{\partial q}{\partial t} = -J(\psi, q) - f_0 \frac{\partial}{\partial p} \frac{\dot{Q}R}{s c_p} + \mathbf{k} \cdot \nabla \times \mathbf{F},$$

where R is the ideal gas constant, c_p is the specific heat at constant pressure, and s is the static stability parameter, and

$$q = \nabla^2 \psi + \beta y + f_0^2 \frac{\partial}{\partial p} \frac{1}{s} \frac{\partial \psi}{\partial p},$$

where ψ is the geostrophic streamfunction and β is the meridional gradient of planetary vorticity evaluated at 45° . The \dot{Q} represents diabatic heating. The \mathbf{F} represents frictional dissipation and has two contributions: a ∇^6 diffusion to remove vorticity at the smallest scales, and a boundary layer contribution described in section 2f.

The quasigeostrophic equations are coupled to an equation for the static stability tendency. This equation is derived from the horizontally averaged thermodynamic equation. The vertical potential temperature fluxes by the zonal mean flow are assumed to be insignificant relative to the eddy fluxes. This assumption can be justified by scaling analysis (Gutowski 1983), and is consistent with two-level model results (Zhou and Stone 1993).

The horizontally averaged potential temperature tendency at time step t is given by

$$\frac{\partial}{\partial t} [\theta_t] = -\frac{\partial}{\partial p} [\omega_t' \theta_t'] + \left[\frac{\dot{Q}_t}{c_p} \right] \left(\frac{p_0}{p} \right)^{R/c_p},$$

where p_0 is the surface pressure and \dot{Q}_t is the diabatic heating at time step t . Primes are used to designate deviations from the zonal mean and $[\]$ indicate a global areal mean. The static stability parameter is calculated from the updated mean potential temperature.

b. Surface air tendency equation

An equation for the surface air temperature tendency is integrated assuming that the fluxes of heat out of the

sea are convergent into the air just at the surface. The vertical wind is assumed to be equal to zero. The sea temperature is held fixed. The turbulent fluxes from the surface air into the first model level are calculated using a flux diffusion approximation. The equation for the surface air temperature tendency (at the level $p_0 - \Delta p/4$) is

$$\frac{\partial T_{sa}}{\partial t} = -J(\psi_{1/2}, T_{sa}) + \dot{Q}_1 + \dot{Q}_2,$$

where $J(\psi_{1/2}, T_{sa})$ is calculated using the streamfunction $\psi_{1/2} = (\psi_0 + \psi_1)/2$, \dot{Q}_1 is the thermal diffusion, and \dot{Q}_2 is the radiative cooling. Here Δp is equal to 1000 hPa/($N - 1$), where N is the number of vertical levels at which temperature is defined in the model.

c. Ekman momentum approximation

Bannon and Salem (1995) used a multiple-scale analysis of the baroclinic Ekman layer to show that the momentum equations used in this model are accurate to $O(E)$. Here E is the Ekman number equal to $2\nu/(fD^2)$, where D is the vertical scale of the flow. These equations will be referred to as the Ekman momentum approximation.

The ageostrophic winds are calculated from the surface shear stress by assuming that the first-order balance in the momentum equation is between the Coriolis force and the vertical diffusion of momentum,

$$\nu_M \rho^2 g \frac{\partial(\mathbf{v}_g + \mathbf{v}_a)}{\partial p} = -c_d \rho_s (\mathbf{v}_g + \mathbf{v}_a).$$

The drag coefficient is equal to the surface drag times the ambient wind, $c_d = c_{\text{surface}} |\mathbf{v}_s|$, and is chosen to be equal to $3 \times 10^{-2} \text{ m s}^{-1}$. The ageostrophic winds are assumed to go to zero above 700 hPa, but in fact the values are only on the order of the geostrophic winds at the first model level and at the surface.

d. Diabatic heating

Diabatic heating is parameterized in this model by a relaxation back to a radiative–convective equilibrium state with a constant diabatic heating timescale. The diabatic heating timescale in the standard model is set equal to 40 days.

The radiative–convective equilibrium state is represented by a horizontally averaged mean lapse rate, dT_e/dz , plus horizontal temperature gradients, dT_e/dy . The lapse rate in radiative–convective equilibrium is chosen to be a constant $-7.0^\circ \text{ km}^{-1}$ in the troposphere. The lapse rate is set equal to zero above the jet maximum. The radiative equilibrium lapse rate would be much larger, closer to $-15^\circ \text{ km}^{-1}$ in the troposphere. Since all moist processes have been neglected in this model, the modification of the radiative equilibrium profile by moist convection is taken into account implicitly by assuming that moisture brings the lapse rate close to a moist adiabat.

The latitudinal temperature distribution is chosen such that the potential temperature gradients are constant with height in the troposphere,

$$\theta(y, p) = -21.5 \sin[\pi(y - L/2)/(L/2)],$$

for $L/4 \leq y \leq 3L/4$, where L is the total channel width—which is set equal to 10 000 km in the standard run—and θ is potential temperature. This gives a temperature contrast of 30° over the center 2500 km of the channel, compared to an estimate of 34° for the wintertime temperature gradients in the lower troposphere from Manabe and Möller (1961). A region with zero temperature gradients is extended 2500 km to the north and south of the sine function to ensure that the channel walls do not modify the dynamics. The gradients in the stratosphere are positive, constant with height, and 10 times smaller than the gradients at 375 hPa.

e. Turbulent heat fluxes in the ABL

The lower boundary is assumed to be a sea surface with fixed temperature, θ_{sea} . A linearized bulk aerodynamic drag formula is used to calculate the surface heat flux,

$$F_{\text{SH}} = -c_d c_p \rho_s (\theta_{\text{air}} - \theta_{\text{sea}}),$$

where ρ_s is the surface density. The surface air temperature θ_{air} is assumed to be equal to the potential temperature at the first level, which in the standard 17-level model is 31 hPa over the surface. The drag coefficient, c_d , is chosen to be equal to $3 \times 10^{-2} \text{ m s}^{-1}$, although in general, the drag coefficient would be a function of the stability.

A diffusive parameterization of turbulent heat fluxes in the ABL are included in the model. Without these fluxes the static stability at the lowest level becomes very large in the equilibrated state because the eddies transport heat vertically, causing the lowest levels to be cold relative to observations. These fluxes are parameterized as

$$F_{\text{SH}} = \nu_T(p) \rho^2 g c_p \frac{\partial \theta}{\partial p} \quad \nu_T(p) = 5 \left(\frac{p}{p_0} \right)^3 \text{ m}^2 \text{ s}^{-1},$$

where p_0 is the pressure at the lower boundary. The heating due to the vertical diffusion of heat is then calculated from the fluxes as

$$\frac{\partial \theta}{\partial t} = \frac{g}{c_p} \frac{\partial F_{\text{SH}}}{\partial p}.$$

f. Friction in the ABL

Friction is parameterized by a linearized bulk aerodynamic drag at the surface and diffusive mixing above the surface, in the same way as was outlined for the diabatic heating.

The linearized bulk aerodynamic drag formula is used to calculate the wind stress at the surface,

$$\boldsymbol{\tau}_s = -c_d \rho_s (\mathbf{v}_g + \mathbf{v}_a).$$

The surface wind is calculated assuming that the temperature at $p = p_s$ is in thermal wind balance with the winds at $p = p_1$ and $p = p_0$. The drag coefficient, c_d , in the standard run is again set equal to $3 \times 10^{-2} \text{ m s}^{-1}$.

Above the surface, the turbulent shear stress is calculated using a flux-gradient formulation,

$$\boldsymbol{\tau}_M = \rho[\mathbf{v}^* \omega^*] = \nu_M(p) \rho^2 g \frac{\partial(\mathbf{v}_g + \mathbf{v}_a)}{\partial p},$$

where

$$\nu_M(p) = 5 \left(\frac{p}{p_0} \right)^3 \text{ m}^2 \text{ s}^{-1}.$$

The vertical diffusion of momentum by the turbulent eddies is then calculated from the shear stress as $\mathbf{F} = g \partial \boldsymbol{\tau}_M / \partial p$.

3. Resolution and domain size dependence of the equilibrated states

In order to determine if the dynamics of the model are convergent at 17 vertical levels, the model has been run using the same parameter values but with twice the vertical resolution. Since it has been found in other studies that the wave that is responsible for the most energy transport may be the largest wave resolved by the model (Cehelsky and Tung 1991), the model has also been run with half the channel length and a quarter of the channel length of the standard run, using the same resolution as the standard run. Finally, to check the horizontal resolution of the standard run, it was rerun with double the resolution of the standard run, both meridionally and zonally.

a. Horizontal resolution and domain size

Figure 1 shows how the vertically averaged kinetic energy and enstrophy spectra depend on horizontal resolution and domain size. The wavelength of the wave that is responsible for the majority of the potential vorticity and heat transport is approximately equal to 4000 km for all these runs (results not shown). Thus this wave is not saturated in our standard run (cf. Cehelsky and Tung 1991 and Welch and Tung 1998). Figure 1 demonstrates that it is necessary to use a channel length larger than the dominant heat transporting wave to resolve the turbulent cascades, and that the domain size and horizontal resolution of the standard run are adequate to resolve the turbulent cascade.

The temperature structure and zonal wind structure are insensitive to the changes in horizontal resolution and domain size (results not shown). The potential vorticity gradients in the equilibrated state are also insensitive to the changes in horizontal resolution and domain

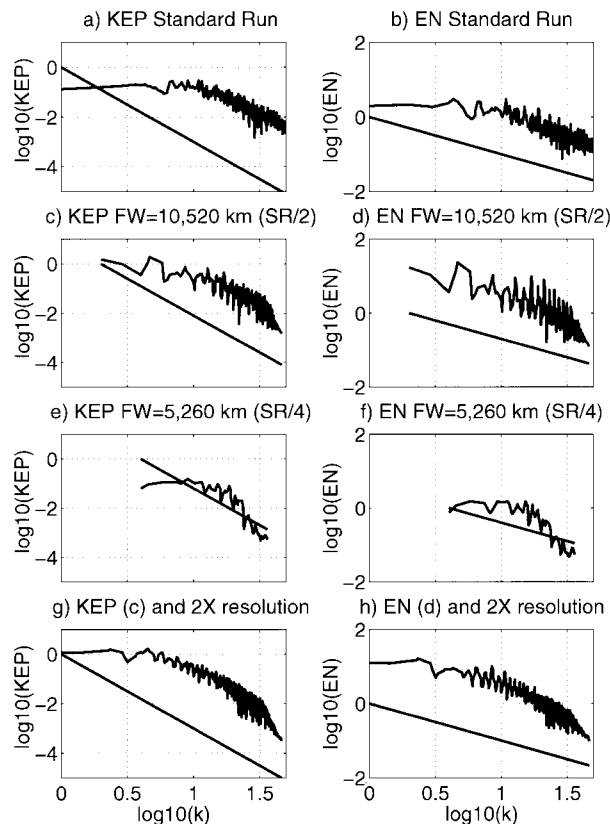


FIG. 1. Vertically and time-averaged eddy kinetic energy, KEP (on the left), and eddy enstrophy spectra, EN (on the right), vs total wavenumber, K , for the horizontal resolution and domain runs (SR, $L/2$, $L/4$, $\Delta X/2$). The vertical and horizontal scales are logarithmic. For comparison lines with slopes of -3 and -1 are shown for the KEP and EN spectra, respectively. (a) and (b) show the results for the standard run; (c) and (d) for one-half the standard domain size; (e) and (f) for one-quarter the standard domain size; and (g) and (h) for twice the standard horizontal resolution.

size below 600 hPa. However, in the upper troposphere the potential vorticity gradients are more sensitive and can differ by up to β .

b. Vertical resolution

An additional run with 33 vertical levels demonstrated that the potential vorticity gradients in the ABL are dependent upon the vertical resolution. This is because it is the mixing of potential temperature and not the mixing of potential vorticity that is the primary dynamic within the ABL. Therefore, the potential vorticity gradients will always be a function of resolution. The potential temperature structure on the other hand is insensitive to the increase in resolution (results not shown).

In previous studies of the impact of variable vertical resolution on the Boussinesq dynamics of a midlatitude β -plane channel model it has been concluded that it is necessary to use at least 10 to 20 levels to resolve the eddy dynamics (Pavan 1996; Hua and Haidvogel 1986).

Our results are consistent with this conclusion. Pavan (1996) also concluded that only 3 levels are necessary to reproduce the general features of the response. The model used by Pavan (1996), however, did not attempt to include thermal diffusion (which dominates the diabatic heating in the ABL) or the feedbacks that maintain the static stability. Lower vertical resolution runs that we carried out showed that including these processes cause the model to be more resolution dependent (results not shown).

4. Equilibrated model climate compared to observations

The standard model run has been chosen to approximate observations of the Northern Hemisphere winter climate as closely as possible, given the simple representations of heating and friction and the construction of the ABL in the model.

a. Distributions of pseudo-potential vorticity

Figure 2a displays the January 1982–94 zonal mean meridional gradient of Ertel's potential vorticity (EPV) divided by the contribution from the planetary vorticity, for the Northern Hemisphere January 1982–94 climatology, produced from the NCEP–NCAR reanalysis dataset. Figure 2a shows that the EPV in midlatitudes is characterized by large gradients below 800 hPa and at the tropopause. Below 800 mb, the meridional temperature gradients are large due to the heating of the atmosphere by the underlying surface. The heating of the air near the surface causes turbulent fluxes of heat and momentum to mix momentum and heat, resulting in small values of static stability near the ground. Large EPV gradients are found at the tropopause where the high EPV stratospheric air meets the low EPV tropospheric air.

The region of EPV homogenization can be seen clearly in Fig. 2a where the EPV gradients between 600 and 750 hPa are less than β . This is the region where the large-scale baroclinically unstable Rossby waves have a critical level. Irreversible mixing of EPV along the isentropes reduces the EPV gradients and the slope of the isentropes in this region. The levels between this region and the tropopause have reduced EPV gradients relative to radiative–convective equilibrium estimates but they are still large relative to β .

Figure 2b displays the potential vorticity gradients, divided by β , for the equilibrated state of the standard run. Comparing the observations, Fig. 2a, to the equilibrated state of the model, Fig. 2b, we see that the qualitative features of the observed potential vorticity distribution are resolved by the model. Quantitatively the potential vorticity gradients in the ABL are larger than the observations.

b. Structure of the mean temperature

Figure 3a compares the static stability of the standard run to observations. Since the eddy diffusion coefficient is a continuous function of height, the large potential vorticity gradients in the ABL extend higher, and the static stability peaks at a higher level than in the observations. The static stability in the standard run below 700 hPa is significantly smaller than in the observations. The magnitude and vertical profile of the static stability above 700 hPa approximate observations.

Model runs that have diffusion coefficients that go to zero below 750 hPa have a much more realistic mean static stability and a larger region of potential vorticity homogenization. The continuous eddy diffusion coefficient has been chosen for the standard run to allow the region over which the vertical eddy heat fluxes play a significant role to depend on the other parameters in the model. Limiting the thermal diffusion to a region closer to the surface would yield a more realistic representation of a thermal capping inversion.

Figure 3b compares the meridional temperature gradients of the standard run to observations. The large thermal damping in the ABL prevents very much reduction of the meridional temperature gradients at the lowest levels by the large-scale eddies. These averaged gradients are seen to be too large relative to the averaged gradients in observations.

Above the ABL, the potential vorticity has been homogenized (Fig. 2b). This homogenization extends along the sides of the jet, where the large-scale waves have a critical level. The homogenization is a result of both increased static stability and decreased horizontal temperature gradients. This region of homogenization approximates the homogenization of EPV that is seen in observations (Figs. 2a and 2b).

Above the homogenized potential vorticity region, the potential vorticity gradients increase with height and have a maximum at the tropopause (Fig. 2b). In the upper troposphere, the meridional temperature gradients from observations are significantly less than those of the standard run. The dynamics that are responsible for the observed temperature gradients in the upper troposphere are not adequately resolved in this simple process model.

c. Structure of the zonal mean eddy fluxes

The model parameters have been chosen so that the zonal mean eddy sensible heat fluxes of the standard run approximate observations of the Northern Hemisphere wintertime eddy sensible heat fluxes. Therefore, the zonal mean eddy sensible heat fluxes from the model are compared to the zonal mean stationary plus transient eddy sensible heat fluxes of the observations. Sensible heat fluxes will be referred to as heat fluxes in what follows.

Figure 4b shows the zonal mean meridional eddy heat

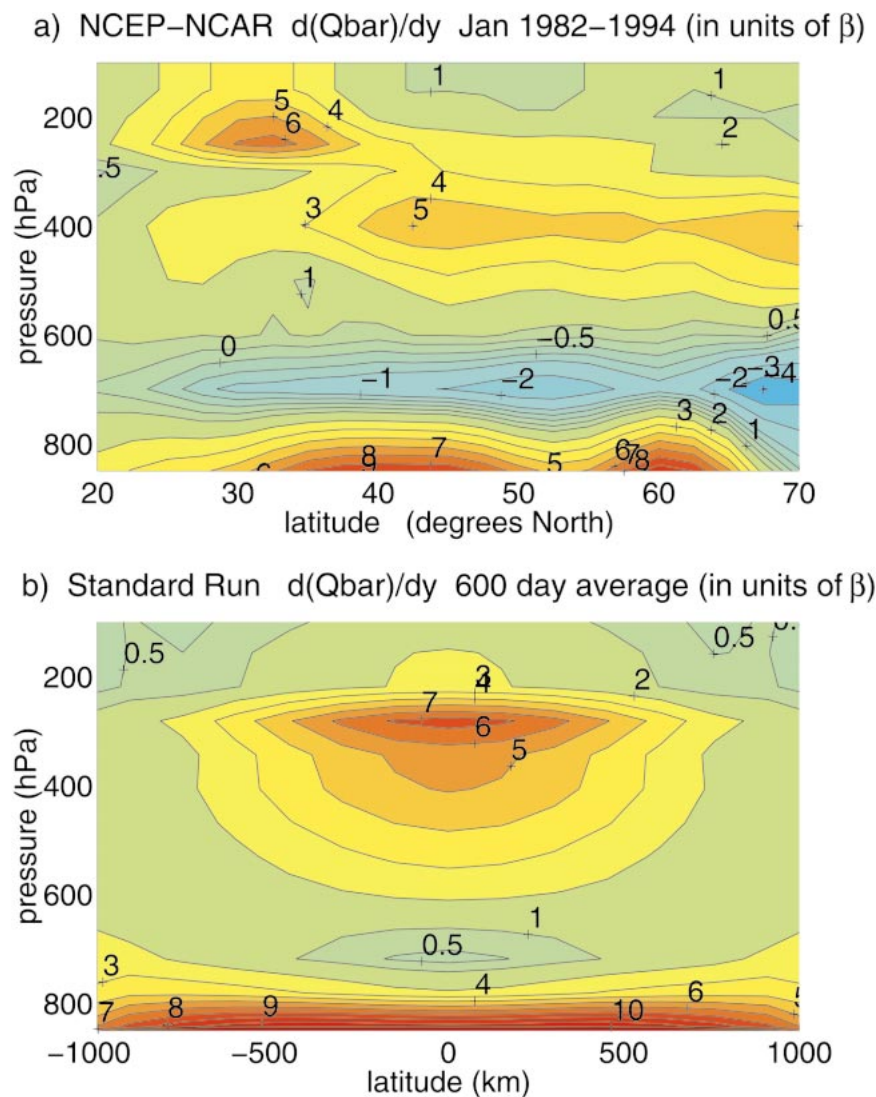


FIG. 2. (a) Zonal mean meridional gradient of potential vorticity (PV) $[-g(f + \zeta)(\partial p/\partial \theta)^{-1}]$ on isentropes, calculated from zonal mean θ , divided by the β contribution to the potential vorticity $[-g\beta(\partial p/\partial \theta)^{-1}]$, for Jan 1982-94. Data from the NCEP-NCAR reanalysis project (Kalnay et al. 1996). (b) Zonal mean meridional gradient of pseudo-potential vorticity divided by β from the equilibrated state of the standard run. Contours of $\pm 0.5 \beta$ have been added to indicate the regions of PV homogenization.

fluxes of the equilibrated standard run and observations. Figure 4a shows the zonal mean vertical eddy heat fluxes, of the equilibrated standard run and observations. The magnitude and vertical structure of the model fluxes resemble the observed fluxes qualitatively. Both the vertical and meridional eddy heat fluxes peak at 875 hPa, due to the thermal damping in the ABL. Without the thermal damping the fluxes peak at the surface. The major inadequacy of the model fluxes is the small secondary peak in the meridional eddy heat flux in the upper troposphere. Since the dynamics of this model are dry, the energy transport due to water vapor fluxes has been neglected. These fluxes are responsible for approximately 35% of the total energy transport in the

lower troposphere (Peixoto and Oort 1992), and their absence contributes to the model's overestimate of the meridional temperature gradients in the lower troposphere.

Figure 4c shows the zonal mean meridional circulation heat fluxes of the equilibrated standard run and observations. The potential temperature transport has been calculated instead of the temperature transport to take into account the cancellation between the sensible heat flux and the potential energy flux. This cancellation is only significant in the mean fluxes since the eddy potential energy flux is small relative to the eddy sensible heat flux (Peixoto and Oort 1992). Given the difference between the two observational datasets, the

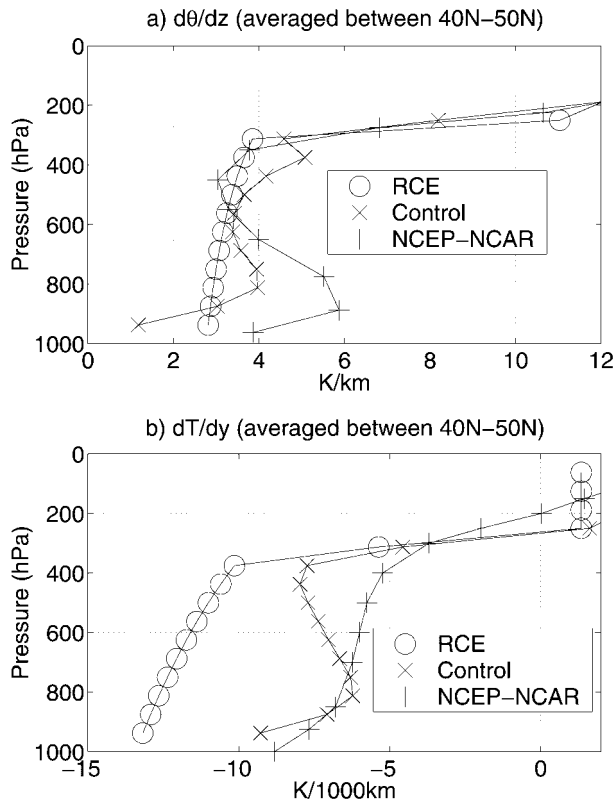


FIG. 3. Comparison of (a) static stability and (b) meridional temperature gradients of the equilibrated state of the standard run with NCEP-NCAR Jan 1982–94 observations.

magnitude and vertical distribution of the model's mean meridional fluxes closely approximate the observed distribution. The vertically integrated mean meridional heat flux in the standard run is much smaller than the vertically integrated eddy heat flux ($-3 K m s^{-1}$ vs $+16 K m s^{-1}$), just as in the observations.

Figure 4d shows the zonal mean eddy momentum fluxes for the standard run compared to observations. This figure shows that the model results resemble the vertical structure and magnitude of the observations quite well, except at the surface. At the lowest level, the observations have negative momentum fluxes, while the model has positive fluxes.

5. Time evolution to the equilibrated basic state

Figure 5 shows the time evolution of the zonal mean potential vorticity gradients at the center of the channel for the first 60 days of the integration of the standard run. At day 0, the model is in approximate RCE and an eddy perturbation is introduced into the model. During the first 12 days the eddy effects are small, and a symmetric state continues to evolve slowly. Then exponentially growing eddies reach large enough amplitudes that their fluxes start to modify the mean potential vorticity gradients. The modification of the mean flow starts in

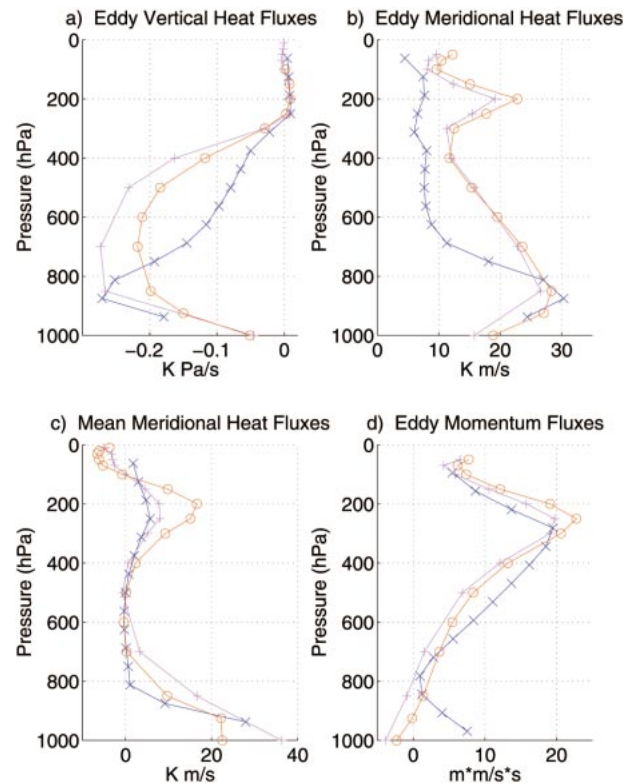


FIG. 4. Comparison of (a) eddy vertical heat fluxes (b) eddy meridional heat fluxes (c) mean meridional heat fluxes (d) eddy momentum fluxes of the equilibrated state of the standard run (\times) with Jan NCEP-NCAR (\circ) 1982–94 and ECMWF ($+$) 1985–89 datasets.

the ABL with an increase in the magnitude of the potential vorticity gradients at the surface and a decrease at the top of the ABL, approximately 700 hPa. This adjustment is due to the vertical eddy heat transports that cool the surface and heat the upper region of the ABL. The efficient mixing of potential temperature due to fluxes across the air–sea interface heats the lower part of the ABL causing the static stability to become very small there. This decrease in the static stability increases the slope of the isentropes and increases the potential vorticity gradients. In the upper region of the ABL the vertical eddy fluxes of heat reduce the slope of the isentropes and decrease the potential vorticity gradients. The wave–mean flow adjustment propagates upward as the eddies become deeper. The flow becomes approximately steady at day 30.

The amplitude of the perturbation potential vorticity becomes steady when the potential vorticity mixing reaches a maximum in the midtroposphere. The equilibrated perturbation potential vorticity has a primary peak at the surface and a secondary peak at the tropopause (figure not shown). There is a minimum in the lower troposphere where the potential vorticity gradients have been homogenized. The flow becomes approximately steady at day 30. The evolution is consistent with the picture suggested by Stone and Nemet (1996)—

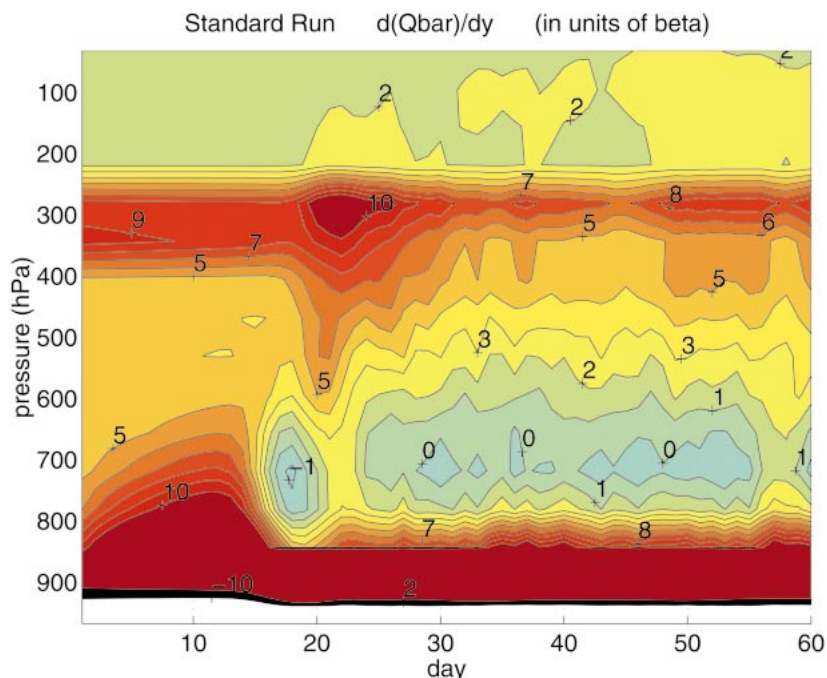


FIG. 5. Time evolution of the zonal mean potential vorticity gradients at the center of the channel from the RCE state to the equilibrated state from the standard run, in units of β .

that is, the baroclinic eddies effectively homogenize the potential vorticity field in midlatitudes in the lower troposphere—but this outcome is prevented in the ABL by diffusion and dissipation, and the upper troposphere remains near radiative–convective equilibrium.

6. Maintenance of the perturbation potential vorticity in the equilibrated state

The balance of terms in the perturbation potential enstrophy tendency equation clearly shows the eddy feedbacks that are maintaining the wave activity. This equation is derived by multiplying the equation for the perturbation potential vorticity tendency by the perturbation potential vorticity. The equation is

$$\frac{1}{2} \frac{\partial \overline{q'^2}}{\partial t} = \overline{v'q'} \frac{\partial \overline{q}}{\partial y} - \frac{1}{2} \frac{\partial \overline{v'q'^2}}{\partial y} + q' \left[-f_0 \frac{\partial}{\partial p} \left(\frac{g}{\pi} \frac{\partial}{\partial p} \rho v_T \frac{\partial \theta}{\partial z} + \frac{\dot{Q}R}{spC_p} \right) + \mathbf{k} \cdot \nabla \times \mathbf{F} \right],$$

where v is the meridional wind, π is the Exner function, primes designate deviations from the zonal mean, and a bar designates a zonal mean.

Perturbation potential enstrophy is equivalent to the squared magnitude of the potential vorticity anomalies. The terms in the perturbation potential enstrophy tendency equation indicate which processes are responsible for the maintenance of the anomalies. The first term on the right-hand side is the quasi-linear flux of potential

vorticity and will be referred to as the downgradient transport of perturbation potential vorticity because the correlation between the mean potential vorticity flux and the mean potential vorticity gradients tends to be negative. Therefore, this term can be thought of as the downgradient transport of perturbation potential vorticity that reduces the mean potential vorticity gradients and is a source of perturbation potential vorticity. The second term on the right-hand side includes the flux of perturbation potential vorticity by wave–wave interactions. The last large expression on the right-hand side consists of the vertical diffusion of heat, Newtonian cooling, and the vertical diffusion of momentum, respectively. All of these act to damp out the perturbation potential vorticity, except for the thermal diffusion at the second model level due to the large decrease in the static stability.

A plot of the terms in the perturbation potential enstrophy tendency equation for the standard run is shown in Fig. 6. This figure shows that the nonlinear wave–wave interactions become significant above the boundary layer. The balance of terms in the perturbation potential enstrophy equation shows that the nonlinear cascade of perturbation potential vorticity and the damping terms contribute equally to balancing the quasi-linear potential vorticity transport between 500 and 600 hPa. Within the ABL the dynamical balance is between the quasi-linear potential vorticity transport and the forcing (which is dominated by the thermal diffusion). The nonlinear wave–wave cascade is insignificant within the

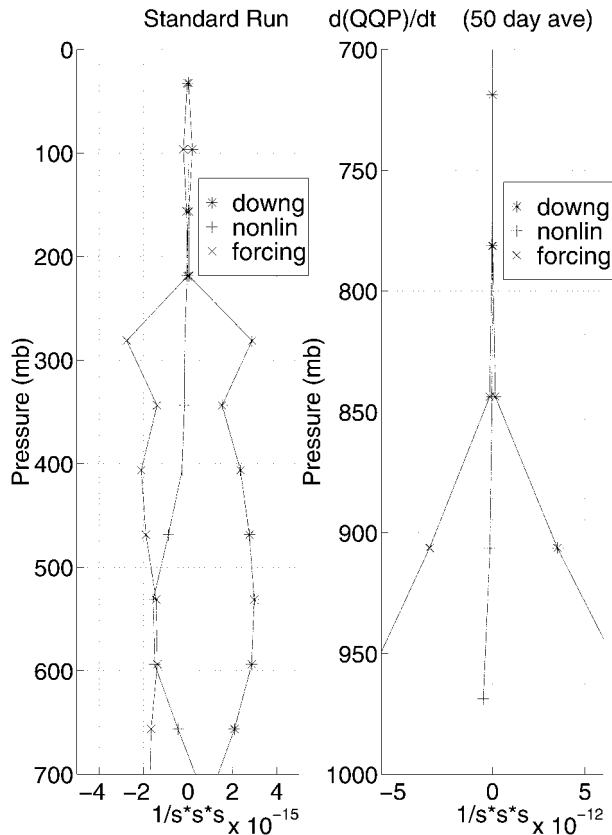


FIG. 6. Terms in the perturbation potential enstrophy tendency equation for the standard run for (a) above the ABL and (b) within the ABL.

ABL, and the dynamics are essentially thermally dissipating Rossby waves as discussed by McIntyre and Norton (1990).

Figure 7 shows the time evolution of the zonal mean potential vorticity gradients above the ABL from the RCE state to the equilibrated state. Figure 7 shows that the zonal mean potential vorticity gradients above the ABL become homogenized within 5 days of when the eddies become finite amplitude (approximately day 15). Around day 30 the potential vorticity gradients at the tropopause become quasi-steady (results not shown). The jet fluctuates about the channel center and has potential vorticity gradients that range between 4 and 6β .

Figure 8 shows the time evolution of the amplitude of the perturbation potential vorticity for waves 1–10 from the standard run. This figure shows that wave 6 dominates in the initial phase of the evolution of the eddy regime, and that its initial growth is consistent with standard models for the most unstable wave of realistic symmetric states. However, in the equilibrated eddy regime, waves 4 and 5 dominate, with wave 4 being somewhat larger.

The adjustment from the symmetric state to the equilibrated state occurs over a very short period, approximately 5 days. Therefore, if the external forcing changes

on timescales of a week or longer, the eddies will have time to adjust the equilibrated state through wave–mean flow adjustment.

7. Nonlinear versus quasi-linear equilibrations

In order to isolate the importance of resolving the nonlinear cascade, a separate experiment was carried out, with the static stability held fixed at the equilibrated static stability of the standard run, with only advective terms that modify the zonal mean flow retained in the tendency equations, and with only wave numbers 4 to 6 retained. We refer to this experiment as the quasi-linear run. Therefore in this run, waves 4, 5, and 6 can directly modify the mean flow but can only modify themselves indirectly through changes in the zonal mean flow. The initial state of the quasi-linear run has meridional temperature gradients equal to the radiative–convective equilibrium meridional temperature gradients of the standard run and static stability equal to the equilibrated static stability of the standard run.

Figure 9 shows the equilibrated zonal mean potential vorticity gradients from the quasi-linear run (cf. the equilibrated zonal mean potential vorticity gradients from the standard run Fig. 2b). It is seen that the homogenization of potential vorticity above the boundary layer in the quasi-linear run is simulated without the nonlinear cascade. This is because most of the adjustment above the ABL is due to the increase in the static stability there (figure not shown), and very little adjustment by the meridional heat fluxes is needed to completely eliminate the potential vorticity gradients above the ABL. The main difference between zonally averaged potential vorticity gradients of the two runs is that the homogenized region is broader in SR.

A Fourier decomposition of the time evolution of the perturbation potential vorticity shows that the quasi-linear run is essentially maintained by wave 5, since the wave 4 perturbation potential vorticity decays away (figure not shown) and wave 6 is always small. Thus given the static stability, wave 4 in SR has to be maintained by the upscale energy cascade. This contrasts with the two-layer model results of Whitaker and Barcilon (1995), who found that the dominant wave is maintained by baroclinic generation.

Two further runs were carried out to determine how different the equilibrated state would be if the maintenance of the equilibrated state was strictly due to either wave 4 or wave 5; that is, these two runs retain only wave 4 or wave 5, respectively. They started from the same initial condition as the quasi-linear run. Comparing these runs and the quasi-linear run to SR it is possible to determine whether the fully nonlinear run equilibrates to a state determined mainly by wave 4, wave 5, or possibly something completely different. Figure 10 shows the difference between the potential vorticity gradients in SR and in the wave 4 only and wave 5 only runs, at the center of the channel. Also shown is the

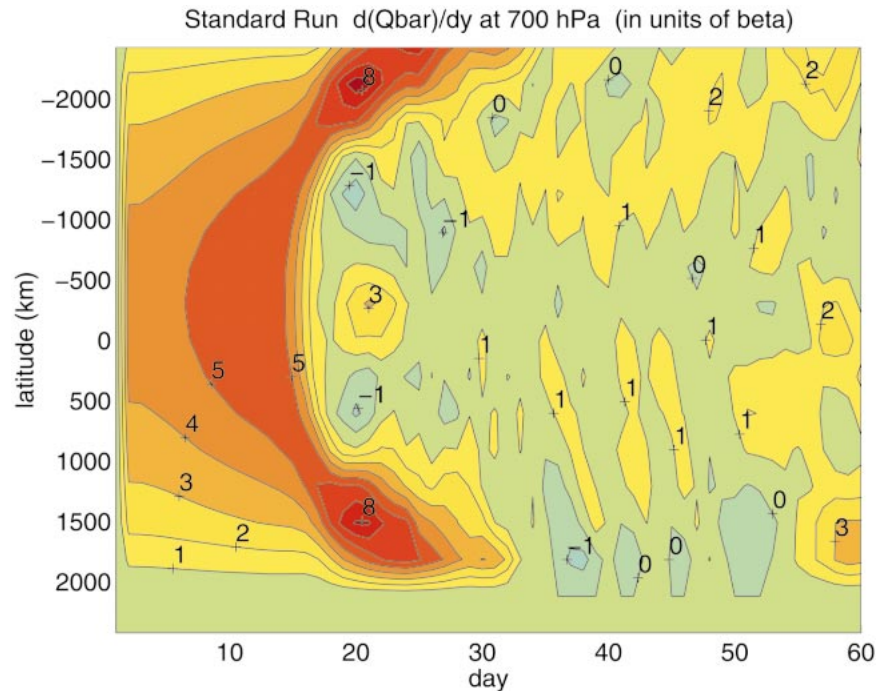


FIG. 7. Time evolution of the zonal mean potential vorticity gradients at 718.75 hPa from the RCE state to the equilibrated state from the standard run, in units of β .

difference in this quantity between SR and its initial value in the wave 4 or 5 only runs. Thus comparing the three curves in Fig. 10 shows us how much the potential vorticity gradients in the wave 4 and wave 5 only runs have changed from their initial conditions, and how much they differ from SR. We see that the wave 4 only run hardly modifies the mean flow, and is quite far from the SR result. In addition we see that the structure of

the potential vorticity gradients above the ABL in SR is closely equal to the equilibrated potential vorticity gradients in the wave 5 only run. Within the ABL the equilibrated potential vorticity gradients from SR are somewhere between the equilibrated potential vorticity gradients due to wave 4 or wave 5 only.

A comparison of the time evolution of the meridional eddy heat fluxes from SR and the wave 5 only run at 875 and 250 hPa, the primary and secondary eddy heat flux maxima, shows that the magnitudes are equivalent but that the wave 5 only run has much larger and more regular oscillations at 875 hPa (figure not shown). This demonstrates that the mean fluxes due to wave 5 approximate those from the fully nonlinear run. The wave 4 only run was found to have fluxes that were approximately 2 times smaller than SR (figure not shown). In addition, a Fourier decomposition of the SR run (not shown) found that both the vertical and meridional eddy heat fluxes in SR are dominated by wave 5. Thus we conclude that the equilibrated state in SR is maintained primarily by the interaction of wave 5 with the zonal mean flow.

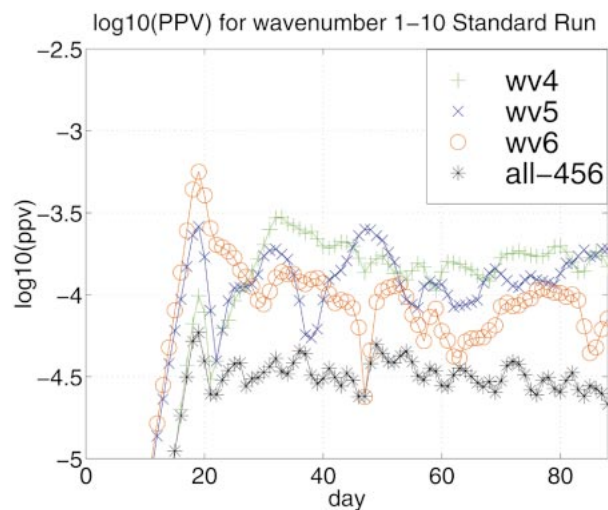


FIG. 8. Time evolution of the amplitude of the perturbation potential vorticity for wavenumbers 1–10 from the standard run. “All-456” shows the amplitude contained in all wavenumbers other than 4, 5, and 6.

8. Stability characteristics of the equilibrated state

This section looks at the role of instabilities in the maintenance of the equilibrated state. First we describe some more properties of the equilibrated state. Changes in the total domain-averaged eddy kinetic energy remain small in the equilibrated state even though the model is

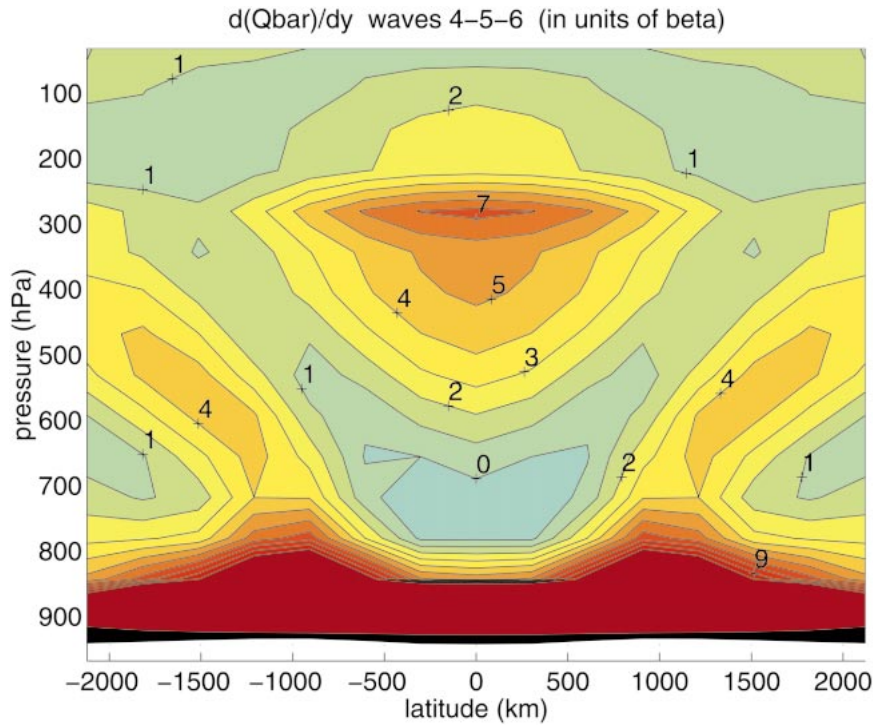


FIG. 9. Latitude–pressure cross section of the zonally averaged potential vorticity gradients in the equilibrated state of the quasi-linear run, in units of β .

clearly not steady (figure not shown). Figure 11 shows a comparison of the eddy kinetic energy (KEP), the zonal mean wind (UM), and the mean potential vorticity gradients (QY) for the first 130 days of the standard run at 281 hPa. The UM and QY are normalized by their initial values, 41.3 m s⁻¹ and 8.2 β , respectively, while KEP is normalized by the maximum value during this period, 444 m² s⁻², so that the fields can be easily com-

pared. This figure shows that at the tropopause there is a clear negative correlation between QY and KEP. The maximum correlation is at a zero time lag. The mean potential vorticity gradients are a minimum (maximum) when the eddy kinetic energy is a maximum (minimum). Therefore, the changes to the zonal mean state at the

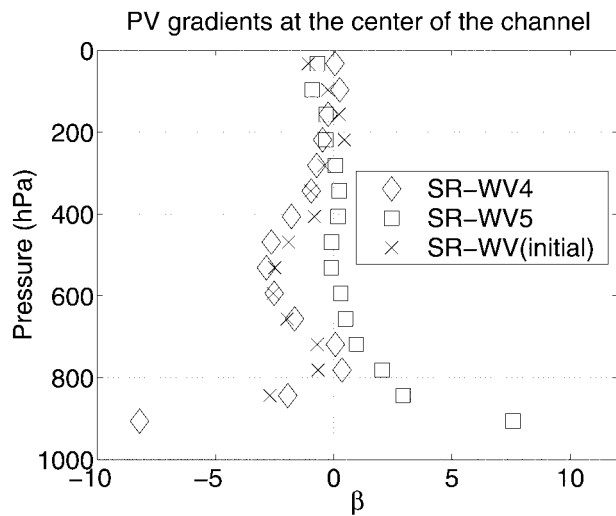


FIG. 10. Comparison of the potential vorticity gradients at the center of the channel in the equilibrated state of the standard run with the quasi-linear runs, in units of β .

Evolution at the center of the channel at 281 hPa

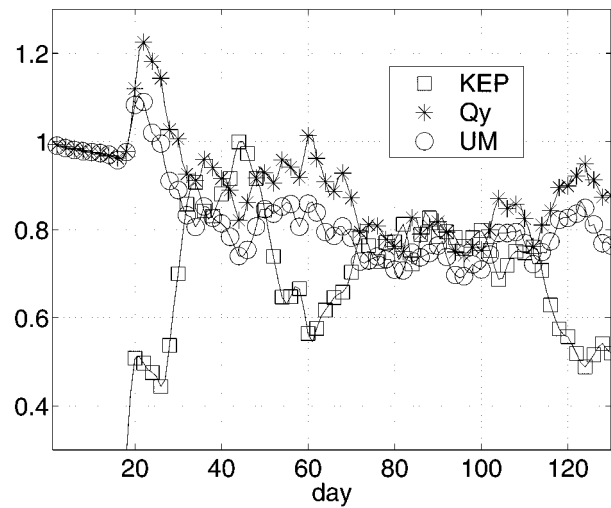


FIG. 11. Time evolution of the eddy kinetic energy (KEP), the zonal mean wind (UM), and the meridional gradient of potential vorticity (QY) at 281 hPa at the center of the channel from the standard run for days 1–130. Scaling is described in the text.

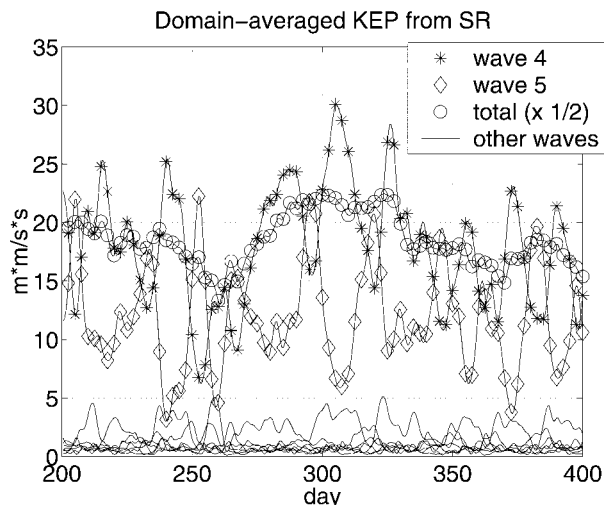


FIG. 12. Domain-averaged time evolution of the total KE and KE per wavenumber at the center of the channel from the standard run for days 200–400. In units of $\text{m}^2 \text{s}^{-2}$.

tropopause occur out of phase with the changes in the eddy kinetic energy. There is a clear positive correlation between the magnitude of the zonal mean wind and the mean potential vorticity gradients at the tropopause. The magnitude of the zonal mean wind at the tropopause, but not the meridional structure of the zonal mean wind, is highly correlated with the time evolution of the magnitude of the potential vorticity gradients at the jet. This result suggests that the barotropic governor proposed by James (1987) is not an important mechanism for the stabilization of the waves during this time, in agreement with the baroclinic turbulence study of Welch and Tung (1998).

Figure 12 shows the total domain-averaged KE and the KE contributed to the domain average by each wavenumber. Figure 12 clearly shows that waves 4 and 5 are responsible for the majority of the KE and that they are highly anticorrelated. All other waves contribute very little to the total domain-averaged KE. Comparing the total KE and its growth rates to those calculated for wave 4 alone, it is clear that large changes in KE due to waves 4 and 5 cancel keeping the changes in the total KE small. The correlation coefficients at zero time lag between the growth rate of the total KE and the growth rate of waves 4 and 5 are 0.19 and 0.22, respectively. The correlation coefficient at zero time lag between the growth rate of total KE and waves 4 and 5 together is 0.74. Therefore, the *joint* response of waves 4 and 5 plays an important role in the variance of KE in SR.

In order to get a sense of whether or not instability is playing a role in the maintenance of the equilibrated mean state, three-dimensional linear stability analyses (3DLSAs) were carried out. All of the forcings used in the fully nonlinear model are linear and are therefore included in the 3DLSAs. The full model is linearized

about various basic states calculated from instantaneous basic states from the standard run following Jin and Hoskins (1995). The static stability is held fixed at the values calculated from the composite basic states. Composites were made for the period between days 200 and 400. One 3DLSA was carried out that linearized the model about the two-dimensional zonal mean time mean state without waves. This composite was found to be linearly stable with the least damped mode being wave 6.

An additional 3DLSA was then run with the basic state taken to be the same two-dimensional zonal mean state plus wave 4. The phase speed of the wave was calculated by averaging the phase speed of the wave between days 200 and 400 from SR. The average phase speed for wave 4 was 2.5 m s^{-1} . The average phase speed was found to be the same at 720 and 218 hPa and showed little variance throughout the integration (figure not shown). The stability analysis was carried out in the reference frame moving with the wave included in the basic state (Lin 1980). Although this state is, strictly speaking, not a solution of the time mean equations, we carried out this 3DLSA in an attempt to gain insight as to how wave 5 might be generated in SR. This state was also found to be linearly stable. The least-damped normal mode was dominated by wave 5.

Finally we carried out a third 3DLSA, in which the basic state is a composite of the instantaneous states when wave 4 was a maximum in SR. Again, this basic state is not strictly a solution of the mean equations, but in this case it is at least a state with zero initial tendency, so that the 3DLSA should show whether there is any initial normal-mode growth. In this case there was. The mode was dominated by wave 6, and had a growth rate of 0.17 day^{-1} . This mode represents an instability of wave 4, since when this 3DLSA was repeated with wave 4 removed from the basic state, it was no longer unstable. This instability is one likely source of wave 6, which is the third-largest wave present in SR.

These results suggest the following scenario for the processes that control the growth and decay of the waves in the model. When wave 4 is a minimum the flow is stable and the energy cascades upscale, particularly from wave 5 to wave 4, so that wave 4 grows and wave 5 decays. Eventually, wave 4 becomes large enough so that the flow becomes unstable and the growth of the waves is dominated by wave 6. This wave quickly saturates (see Fig. 12), and gives up its energy to larger scales. The growth of wave 5 while wave 4 is decaying (see Fig. 12) suggests that in effect the energy that wave 6 extracts from wave 4 by linear instability is then supplied to wave 5 by nonlinear wave–wave interactions. Once wave 4 has become small enough, the flow becomes stable, wave 5 now loses energy to wave 4, so wave 5 decays and wave 4 grows, and the cycle repeats itself. The interaction between wave 4 and 5 in SR suppresses the much larger oscillations in KE seen in the wave 5 only run described in section 6, but in both cases

the mean properties of wave 5 and its interaction with the mean flow are very similar, so the mean equilibrated states are similar in both runs.

9. Discussion

The results of this study suggest an equilibrated state that is in many ways similar to the midlatitude troposphere. This equilibrated state is maintained by quasi-linear dynamics and can be thought of as a quasi-neutral state. This neutral state can best be understood in terms of a coupling between the efficient vertical mixing of potential temperature in the ABL with the efficient meridional mixing of potential vorticity in the lower troposphere. This is very significant in two aspects. First, changes in the surface temperature will be reflected in the potential temperature at the top of the ABL, which provides a boundary condition for the mixing of potential vorticity in the free troposphere. Therefore, changes in the surface temperature may significantly impact the temperature structure of the free troposphere. Second, this study suggests that the efficient homogenization of potential vorticity near the steering level may be a robust feature of the equilibrated state, that is, insensitive to changes in forcing. Both of these aspects will be explored in two companion papers that look at the sensitivity of the model's equilibrated state to changes in forcing and dissipation.

Our study suggests a novel scenario of equilibration due to wave–mean flow interaction. The total growth rate of the eddy kinetic energy was found to be essentially determined by the feedback between wave 5, which was responsible for the majority of the wave–mean flow fluxes, and wave 4, which was the wave with the largest amplitude and depends on the upscale energy cascade for its existence. The equilibrated state's zonal mean state was found to be linearly stable, but it was linearly unstable part of the time when a sufficiently large wave 4 component was present and was added to its zonal mean basic state. The most rapidly growing mode in the linear stability analysis about the wavy basic state was found to be dominated by a wave 6. From our results it appears that the variance in the fully nonlinear run was maintained in part by the feedback between the energy cascade to the larger scales and the extraction of energy from the larger-scale waves by shorter linearly unstable waves. Linearizing about the zonal mean basic state overestimates the stability of the equilibrated state, and excludes this significant mechanism. The wave–wave fluxes appear to play a different role than in the Welch and Tung (1998) saturation scenario. First, wave 5 is responsible for the majority of the wave–mean flow fluxes in part because shorter waves saturate, but also in part because it can draw energy from wave 4 with the aid of smaller-scale instabilities. Second, even though there is a nonlinear cascade and an energy transfer to larger scales, the equilibrated state of the fully nonlinear run was shown to closely approximate the

neutral state of the wave 5 only run. The nonlinear wave–wave fluxes were shown to play a significant role in the equilibration by increasing the amplitude of wave 4. This in turn appears to cause a mode dominated by wave 6 to become linearly unstable.

The episodic growth of waves 4 and 5 in the equilibrated state appears to be consistent with Farrell's (1985) picture of baroclinic eddy growth associated with nonnormal modes. Wave–wave interactions are essential in giving rise to these waves; nevertheless both draw on the mean available potential energy and transport heat poleward, and we could find no normal modes that could by themselves account for their growth. However, the equilibrated state also contains eddies (primarily wave 6) that appear to grow because of normal-mode instability, and these appear to facilitate the exchange of energy between waves 4 and 5. Thus the equilibration involves a mixture of Farrell's mechanism and the classic mechanism of normal-mode instability, although, to be sure, it is a wave instability rather than an instability of the zonal mean flow. This more complicated picture is likely to be sensitive to the particular parameter choices we have made, and we plan to investigate its dependence on the parameters in subsequent papers.

The results of this study are consistent with the results of Simmons and Hoskins (1978) where the reduction of lower-tropospheric temperature gradients due to baroclinic growth preceded the modification of the jet structure due to barotropic decay in the life cycle of a nonlinear baroclinic eddy. This study extends the studies of eddy life cycles to a fully equilibrated state that is forced by both heating and friction, and in which eddies are always present. The results of this study suggest an equilibrated state that may be relevant to dynamics in the atmosphere.

The equilibrated state in our model has a vertical structure consistent with the suggestion of Stone and Nemet (1996) that the vertical structure of the potential vorticity (PV) gradients in the midlatitude troposphere has distinct regimes: a region of large PV gradients within the ABL and a region of approximately homogenized PV between 600 and 750 hPa. The results of this model study have demonstrated how these regimes come about in one particular set of circumstances. How these results depend on the forcing and dissipation will also be explored in the companion papers referred to earlier. However, they do show that the results of the two-layer models, which cannot resolve these different regimes, need to be treated with caution.

Acknowledgments. This work was supported in part by the Global Atmospheric Modeling and Analysis Program of the National Aeronautics and Space Administration, directed by Ken Bergman, under Grant NAG5-4880 to MIT. We are indebted to Richard Lindzen for many useful discussions. The International Pacific Research Center is partly sponsored by Frontier Research System for Global Change.

REFERENCES

- Bannon, P. R., and T. L. Salem Jr., 1995: Aspects of the baroclinic boundary layer. *J. Atmos. Sci.*, **52**, 574–596.
- Cehelsky, P., and K. K. Tung, 1991: Nonlinear baroclinic adjustment. *J. Atmos. Sci.*, **48**, 159–172.
- Farrell, B., 1985: Transient growth of damped baroclinic waves. *J. Atmos. Sci.*, **42**, 2718–2727.
- Fullmer, J. W. A., 1982: Calculations of the quasi-geostrophic potential vorticity gradient from climatological data. *J. Atmos. Sci.*, **39**, 1873–1877.
- Gutowski, W. J., 1983: Vertical eddy heat fluxes and the temperature structure of the mid-latitude troposphere. Ph.D. thesis, Massachusetts Institute of Technology, 294 pp. [Available from Document Services, MIT, 160 Memorial Drive, Cambridge, MA 02139.]
- , L. E. Branscome, and D. A. Stewart, 1989: Mean flow adjustment during life cycles of baroclinic waves. *J. Atmos. Sci.*, **46**, 1724–1737.
- Hua, B. L., and D. B. Haidvogel, 1986: Numerical simulations of the vertical structure of quasi-geostrophic turbulence. *J. Atmos. Sci.*, **43**, 2923–2936.
- James, I., 1987: The suppression of baroclinic turbulence in horizontally sheared flows. *J. Atmos. Sci.*, **44**, 3710–3720.
- Jin, F. F., and B. J. Hoskins, 1995: The direct response to tropical heating in a baroclinic atmosphere. *J. Atmos. Sci.*, **52**, 307–319.
- Kalnay, E., and Coauthors, 1996: The NCEP/NCAR 40-Year Reanalysis Project. *Bull. Amer. Meteor. Soc.*, **77**, 437–471.
- Lin, C. A., 1980: Eddy heat fluxes and stability of planetary waves. Part I. *J. Atmos. Sci.*, **37**, 2353–2372.
- Lindzen, R. S., 1993: Baroclinic neutrality and the tropopause. *J. Atmos. Sci.*, **50**, 1148–1151.
- Manabe, S., and F. Möller, 1961: On the radiative equilibrium and heat balance of the atmosphere. *Mon. Wea. Rev.*, **89**, 503–532.
- McIntyre, M. E., and W. A. Norton, 1990: Dissipative wave–mean flow interactions and the transport of vorticity or potential vorticity. *J. Fluid Mech.*, **212**, 403–435.
- Morgan, M. C., 1994: An observationally and dynamically determined basic state for the study of synoptic scale waves. Ph.D. thesis, Massachusetts Institute of Technology, 123 pp. [Available from Document Services, MIT, 160 Memorial Drive, Cambridge, MA 02139.]
- Pavan, V., 1996: Sensitivity of a multi-layer quasi-geostrophic β -plane channel to the vertical structure of the equilibrium meridional temperature gradient. *Quart. J. Roy. Meteor. Soc.*, **122**, 55–72.
- Peixoto, J. P., and A. H. Oort, 1992: *Physics of Climate*. American Institute of Physics, 520 pp.
- Simmons, A. J., and B. J. Hoskins, 1978: The life cycles of some nonlinear baroclinic waves. *J. Atmos. Sci.*, **35**, 411–431.
- Stone, P. H., 1972: A simplified radiative-dynamical model for the static stability of rotating atmospheres. *J. Atmos. Sci.*, **29**, 405–418.
- , and B. Nemet, 1996: Baroclinic adjustment: A comparison between theory, observations, and models. *J. Atmos. Sci.*, **53**, 1663–1674.
- Sun, D., and R. S. Lindzen, 1994: A PV view of the zonal mean distribution of temperature and wind in the extratropical troposphere. *J. Atmos. Sci.*, **51**, 757–772.
- Welch, T. W., and K. K. Tung, 1998: Nonlinear baroclinic adjustment and wavenumber selection in a simple case. *J. Atmos. Sci.*, **55**, 1285–1302.
- Whitaker, J., and A. Barcilon, 1995: Low-frequency variability and wavenumber selection in models with zonally symmetric forcing. *J. Atmos. Sci.*, **52**, 491–503.
- Zhou, S., and P. H. Stone, 1993: The role of large-scale eddies in the climate equilibrium. Part II: Variable static stability. *J. Climate*, **6**, 1871–1881.